Iraqi Journal of Physics, 2024
https://doi.org/10.30723/ijp.v22i4.1301
Vol. 22, No. 4, PP. 99-106
P-ISSN: 2070-4003
E-ISSN: 2664-5548

Structural Characteristics and Photocatalytic Activity of TiO_2/Si_3N_4 Nanocomposite Synthesized via Plasma Sputtering Technique

Ali N. Munif [1a*] and Firas J. Kadhim[2b]
[1]*Department of Medical Physics, College of Science, University of Warith Alandiyaa, Karbala, Iraq*
[2]*Department of Physics, College of Science, University of Baghdad, Baghdad, Iraq*
[a*] Corresponding author: alinazem574@gmail.com

Abstract

This work evaluates a new titanium dioxide/silicon nitride (TiO2/Si3N4) catalyst prepared by the deposition of thin films of Si3N4 and TiO2 nanostructures on glass using a lab-made closed-field unbalanced DC reactive magnetron sputtering technique. A highly pure silicon sheet and titanium sheet were used as a sputtering target, and a gas mixture of (Ar: N_2) and (Ar:O_2) with mixing ratios of (50:50) for each was used to prepare TiO_2/Si_3N_4 sample, respectively. This sample has been heat treated. The structure and morphology of the catalyst were determined by X-ray diffraction (XRD), Field-Emission Scanning Electron Microscopy (FE-SEM), Energy Dispersive X-ray (EDX) Spectroscopy, and Fourier transform infrared (FTIR) spectroscopy. The resultant nanocomposite sample was polycrystalline, and there were no impurities in the investigated nanocomposite, as revealed by XRD analysis. The absorption edge was found to be at 420 nm, as revealed by UV-visible spectroscopy, and the study of the optical properties also showed that the absorption edge of TiO_2/Si_3N_4 was shifted towards the low energy region (redshift) relative to TiO_2. The results obtained from the photodegradation of organic pollutants under a Xenon lamp indicate that TiO_2/Si_3N_4 nanocomposite photocatalytic activity is significantly more effective than TiO_2 nanophotocatalyst.

Article Info.

Keywords:
Titanium Dioxide, Silicon Nitrite, Nanocomposites, Reactive Sputtering, Photocatalyst.

Article history:
Received: May,19, 2024
Revised: Jul. 17, 2024
Accepted: Aug. 23, 2024
Published:Dec. 01, 2024

1. Introduction

The efficiency of semiconductors as photocatalysts for degrading harmful compounds was recognized when it was established that they could be effectively used to produce products such as H_2 and O_2. There are various extensively used photocatalysts, such as ZnO, CuO, CdS and Fe_2O_3 [1, 2].

Titanium dioxide (TiO_2) is the most prominent photocatalyst [3-5]. It stands out due to its unique alchemical stability, optical, physical and electrical characteristics and applications as a semiconducting material and an excellent photocatalyst [6, 7]. However, in addition to the several advantages listed above, TiO_2 has some disadvantages regarding practical applications. Because of the large band gap, the photocatalytic activity uses only a minimum amount of energy from the near ultraviolet (UV) region of sunlight. As a result, when exposed to sunlight, TiO_2 becomes practically inactive [8, 9]. As a result, researchers have proposed several ways to narrow titanium dioxide's band gap so that it can directly absorb sunlight. One of the most successful methods for enhancing TiO_2 photocatalytic activity under visible light is doping it with non-metals such as carbon, nitrogen, and Sulphur.

Composite materials consisting of silicon nitride (Si_3N_4) and TiO_2 have the photocatalytic capabilities of TiO_2 while also exhibiting great stability from Si_3N_4 in addition to other properties due to the formation of chemical bonds [10]. Composites are becoming important due to many suitable properties, such as modulus, strength, heat deflection temperature, thermal and electrical conductivity, lower thermal expansion coefficient, and low cost [11]. TiO_2/Si_3N_4 can be used to coat stainless steel to prevent it

from oxidation and chemical corrosion, as well as antireflection coatings for optical glasses.

A DC reactive magnetron sputtering technique has been used to synthesize this nanocomposite, although physical vapor deposition (PVD) and chemical vapor deposition (CVD) methods and techniques exist due to their many advantages over other techniques, such as the high purity and optical and structural homogeneity of the produced thin film [12-15].

This study aims to combine the advantages of titanium dioxide and silicon nitride to study a new nanocomposite with excellent photocatalytic properties and large surface area. The surface area of the photocatalyst increases the photodegradation since it contains a greater number of active sites compared to the low surface area materials. The effect of the composition on nanostructure, optical properties and photocatalytic activity in the degradation of organic pollutants was systematically investigated.

2. Experimental Work

Nanocomposite coatings of TiO_2/Si_3N_4 were deposited on transparent borosilicate glass substrates using arc DC reactive magnetron sputtering technique. First, the Si_3N_4 thin film was deposited by reactive sputtering of an n-type silicon target. Secondly, the TiO_2 thin film was deposited on the same substrate by sputtering of a 0.999-purity Ti target. Then, the samples were thermally treated at 100°C. The operation conditions were optimized as the discharge voltage was 2.5 and 3 kV, the gas mixing ratio for (Ar: N_2) and (Ar:O_2) was 50:50, and the discharge current was 40 and 45 mA to deposit Si_3N_4 and TiO_2 films, respectively. The other parameters were: the interelectrode distance was 4 cm, working pressure of 0.085 mbar, and deposition time of 2hrs for TiO_2 and 1h for Si_3N_4. More details on the DC reactive magnetron sputtering system used in this work can be found elsewhere [16, 17].

Photocatalytic activity of TiO_2 and TiO_2/Si_3N_4 (100°C) nanocomposite thin films were investigated through the photodegradation of methylene violet (MV) dye. The aqueous suspension was placed in a dark cabinet and irradiated by UV light at various times. After that, the photocatalytic degradation of pollutants was determined using UV-visible spectrometer.

3. Results and Discussion

XRD measurements were conducted on all samples using the Cu K line with λ = 0.154051 nm. The purpose was to analyze the structure of TiO_2 and TiO_2/Si_3N_4 without and with thermal processing and to determine the variations in mean particle size resulting from thermal processing. Fig. 1 shows the XRD patterns of TiO_2 and TiO_2/Si_3N_4 composite materials without and with thermal processing at a temperature of 100°C. The XRD patterns of TiO_2 thin film showed polycrystalline structures, while TiO_2/Si_3N_4 nanocomposite film samples showed a polycrystalline structure that included the formation of Si_3N_4 microstructure. The peak assigned at 32.4^o belonging to Si_3N_4 structure was only observed in the structure of TiO_2/Si_3N_4 composite [18]. The XRD pattern of TiO_2 showed peaks assigned at 25.36^o, 37.85^o, 48.07^o, 37.62^o, 55.12^o, 63.82^o, 70.42^o, and 75.41^o corresponding to 101, 004, 112, 200, 105, 211, 118, 116, 220, and 125 crystal planes, respectively, as reported in the JCPDS card no. 21-1272. The XRD pattern of TiO_2/Si_3N_4 showed peaks assigned at 27.26^o, 35.90^o, 41.07^o, 43.86^o, 54.1^o and 56.47^o corresponding to 110, 101, 111, 210, 211 and 220 crystal planes, respectively, as reported in the JCPDS card no. 88-1175 [19, 20]. When TiO_2/Si_3N_4 nanocomposite was treated thermally, the intensity of the diffraction peaks in the XRD pattern increased due to crystal growth, and the full width at half maximum (FWHM) decreased.

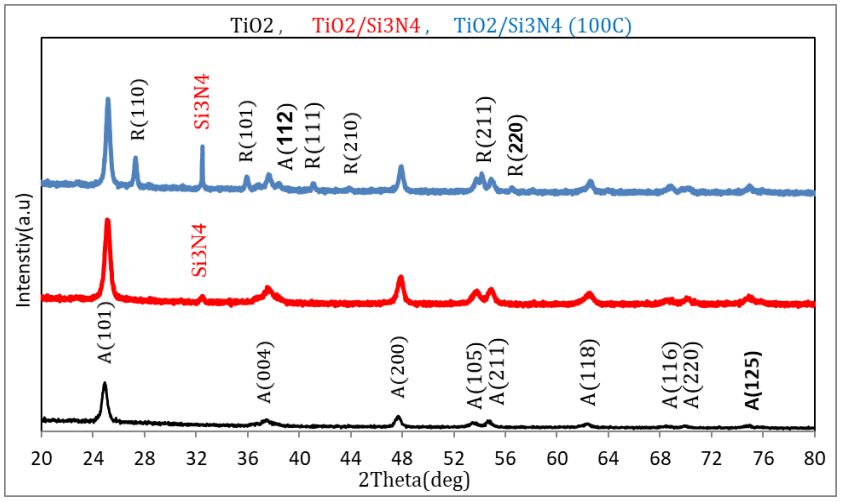

Figure 1: XRD patterns of TiO_2, TiO_2/Si_3N_4 nanocomposite without and with thermal processing at 100℃.

Fig. 2 shows the Fourier-transform infrared (FTIR) spectra of TiO_2, TiO_2/Si_3N_4 nanocomposite materials without and with thermal processing. A band at around 667 cm^{-1} represents the TiO_2 matrixes. While a weak band at 443 cm^{-1} Ti-O corresponds to rutile structure. The bands at 1400 cm^{-1} correspond to Ti-O-Ti bonds in the TiO_2 lattice. For TiO_2/Si_3N_4 nanocomposite thin film, the results at 962.41 and 1085.85 cm^{-1}, which are indexed to the bond's stretching vibration mode, confirmed the formation of Si-N and Si-N-Si bonds [21]. The band at 1630 cm^{-1} corresponds to the bending vibration of the O–H bond, and the broad band around 3400 cm^{-1} corresponds to the stretching mode of the O–H due to water molecules in the atmosphere [22, 23]. A sign of the prepared Si_3N_4 nanostructures' purity may be the absence of specific bands associated with the TiN and SiO_2 molecules.

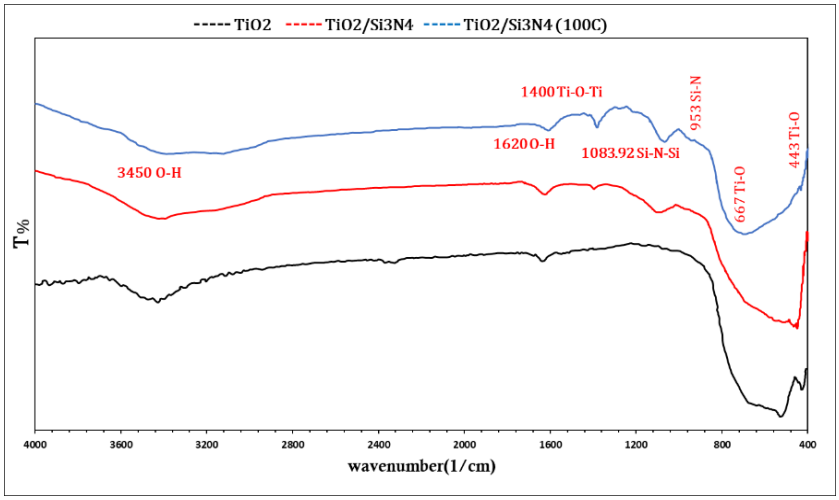

Figure 2: FTIR spectra of TiO_2, TiO_2/Si_3N_4 nanocomposite materials without and with thermal processing at 100℃.

The resultant TiO_2/Si_3N_4 nanocomposite is shown by the Field-Emission Scanning Electron Microscopy (FE-SEM) shown in Fig. 3. The TiO_2/Si_3N_4 particles appeared as nearly uniform spherical, and the average particle size was estimated at around 32.01 nm. The Energy Dispersive X-ray (EDX) spectrum shown in Fig. 4 recorded and analyzed the elemental composition of TiO_2/Si_3N_4 nanocomposites. The existence of Ti, Si, N_2 and O_2 was confirmed. The structure of TiO_2/Si_3N_4 was of high purity and homogeneity, matching the FTIR results. The presence of carbon results from handling the sample within the EDX instrument.

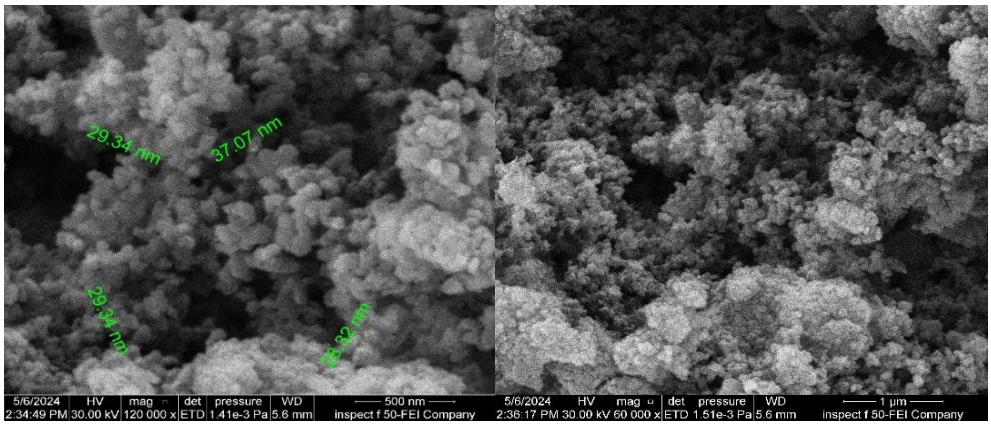

Figure 3: FE-SEM micrographs of TiO_2/Si_3N_4 nanocomposite materials with thermal processing at 100℃.

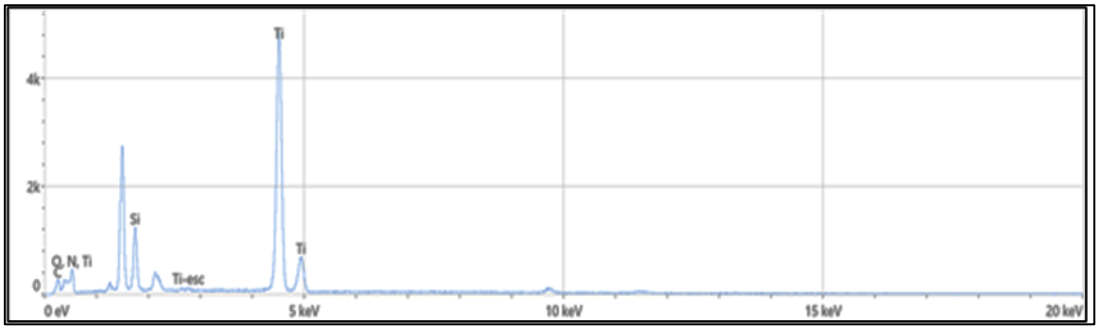

Figure 4: EDX spectrum of TiO_2/Si_3N_4 nanocomposite materials with thermal processing at 100℃.

The UV-visible spectroscopy absorption spectra of the TiO_2 and TiO_2/Si_3N_4 nanocomposite thin films at (100°C) are shown in Fig. 5. The TiO_2/Si_3N_4 (100°C) nanocomposite sample has a greater absorbance than the TiO_2 thin film in the visible spectrum. Fig. 6 shows the relationship between $(\alpha h\nu)^{1/2}$ and photon energy ($h\nu$) used to calculate the energy band gap of the synthesized structures [24]. It was found that the energy bandgap was reduced from 3.2eV for the TiO_2 sample to 2.9eV for the TiO_2/Si_3N_4 (100°C). That is, the absorption edge of the nanocomposite samples was shifted towards the visible region compared with the absorption edge of TiO_2 photocatalyst in the UV region.

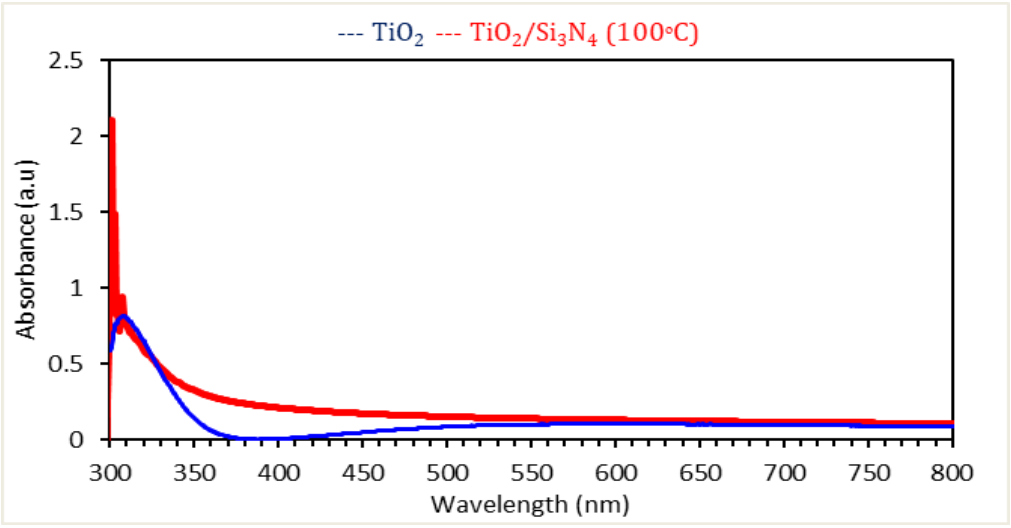

Figure 5: Absorption spectra of TiO_2 and thin film of TiO_2/Si_3N_4 nanocomposite materials with thermal processing at 100°C.

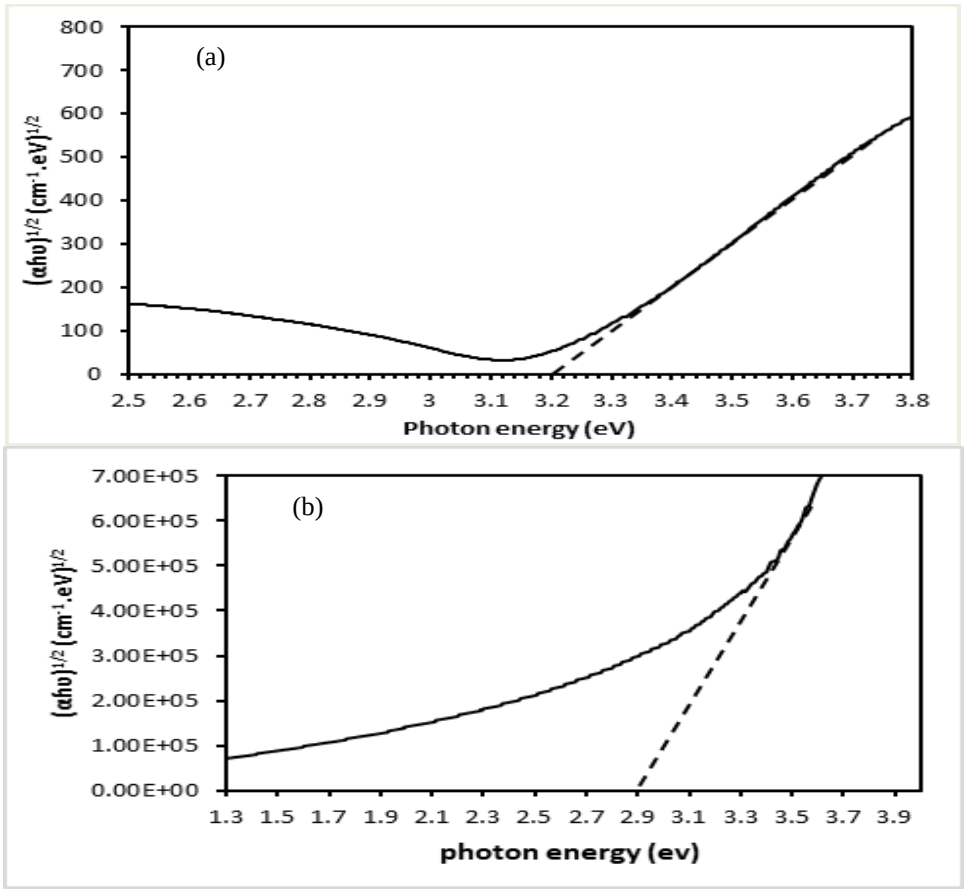

Figure 6: Energy band gap determination of (a) TiO_2 thin film (b) TiO_2/Si_3N_4 nanocomposite materials with thermal processing at 100°C.

The photodegradation efficiency of Methylene Violet (MV) dye as an organic pollutant in an aqueous suspension containing thin film samples under UV light was observed to investigate the photocatalytic activity of TiO_2/Si_3N_4 nanocomposite thin films. The UV-visible absorption spectra of MV dye were recorded as reference spectra corresponding to the initial pollutants concentration ($C_\circ$) in the absence of thin-film samples and UV radiation.

The normalized residual pollutants concentration ($C/ C_\circ$) following degradation was determined using the following formula [25, 26]

$$\frac{c}{c_\circ} = \frac{A_{time=t}}{A_{time=0}} \qquad (\mathbf{1})$$

where $A_{time=0}$ is the initial intensity of the main absorption peak of MV dye and/or polluted water solutions, $A_{time=t}$ is the intensity after exposure time t, $C_\circ$is the initial concentration of MB dye before adding the TiO_2 thin film to the solution, and C is the residual concentration of MV dye after exposure time (t).

Fig. 7(a) shows how the absorbance of the MV dye solution decreased from its original value after 120 minutes of UV radiation exposure. This decrease is attributed to the influence of TiO_2/Si_3N_4 films present inside the MV solutions. Fig. 7(b) depicts typical variation in the normalized residual MV dye concentration ($C/ C_\circ$) as a function of exposure time to UV radiation. The values of the reaction rate constant (k) were determined and listed in Table 1. The reaction rate constant of TiO_2/Si_3N_4 (100°C) was found to be higher than that of TiO_2. Hence, TiO_2/Si_3N_4 at 100°C exhibits better photocatalytic behavior than TiO_2 nanostructure.

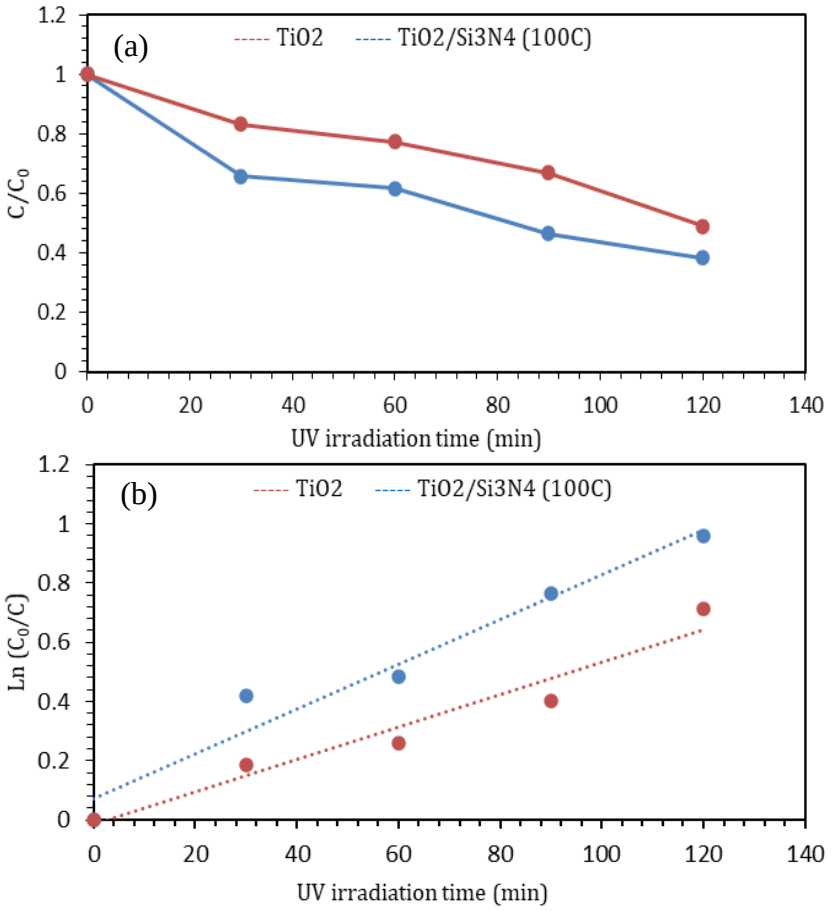

Figure 7: (a) Absorbance decay of methylene blue (MV) dye, and (b)The relation of ln (C_0/C) both versus UV irradiation time for TiO_2 and TiO_2/Si_3N_4 nanocomposite materials with thermal processing at 100 ℃.

Table 1. Reaction rate constant (k) as a function of (Ar：O_2) and (Ar:N_2) mixing ratio for the case of MV dye.

Material	k (min^{-1})
TiO_2	0.005471
TiO_2/Si_3N_4	0.007536

The TiO_2/Si_3N_4 photocatalyst sample that was heat-treated at 100°C is clearly more effective at photocatalysis. This can be explained by the sample's greater ability for light absorption and longer charge carrier lifetime [27, 28].

4. Conclusions

In this study, high-quality TiO_2/Si_3N_4 nanocomposite thin films that have structure purity and optical homogeneity, were synthesized by dc reactive magnetron sputtering technique with thermal treatment. The structural, morphological, and optical properties of the TiO_2 and TiO_2/Si_3N_4 samples indicated the successful preparation of the new nanocomposite. The results of the TiO_2/Si_3N_4 thin film prepared by the reactive DC sputtering were quite reasonable compared to other reported techniques. The Photodegradation results confirmed that the photocatalytic activity of the TiO_2/Si_3N_4 nanocomposite prepared and thermally treated at 100°C was higher than that of the TiO_2 thin film. The photocatalytic activity of the nanocomposite is attributed to the improvement in charge separation.

Conflicts of interest

The authors declare they have no competing interests.

References

1. F. Hasanvandian, A. Shokri, M. Moradi, B. Kakavandi, and S. Rahman Setayesh, J. Hazar. Mat. **423**, 127090 (2022). DOI: 10.1016/j.jhazmat.2021.127090.
2. A. Payan, A. Akbar Isari, and N. Gholizade, Chem. Eng. J. **361**, 1121 (2019). DOI: 10.1016/j.cej.2018.12.118.
3. B. Alshabander and A.-A. Mays Bassim, Iraqi J. Phys. **21**, 10 (2023). DOI: 10.30723/ijp.v21i1.1042.
4. R. Krakowiak, J. Musial, P. Bakun, M. Spychała, B. Czarczynska-Goslinska, D. T. Mlynarczyk, T. Koczorowski, L. Sobotta, B. Stanisz, and T. Goslinski, Appl. Sci. **11**, 8674 (2021). DOI: 10.3390/app11188674.
5. E. A. Elgohary, Y. M. A. Mohamed, H. A. El Nazer, O. Baaloudj, M. S. S. Alyami, A. El Jery, A. A. Assadi, and A. Amrane, Catalysts **11**, 1498 (2021). DOI: 10.3390/catal11121498.
6. C. Thambiliyagodage, Envir. Nanotech. Monit. Managem. **16**, 100592 (2021). DOI: 10.1016/j.enmm.2021.100592.
7. A. Bahadoran, J. R. De Lile, S. Masudy-Panah, B. Sadeghi, J. Li, M. H. Sabzalian, S. Ramakrishna, Q. Liu, P. Cavaliere, and A. Gopinathan, J. Manuf. Mater. Process. **6**, 69 (2022). DOI: 10.3390/jmmp6040069.
8. A. Fujishima and X. Zhang, Comp. Rend. Chim. **9**, 750 (2006). DOI: 10.1016/j.crci.2005.02.055.
9. S. Ahmed, M. G. Rasul, W. N. Martens, R. Brown, and M. A. Hashib, Wat. Air Soil Pollut. **215**, 3 (2011). DOI: 10.1007/s11270-010-0456-3.
10. M. K. Ali and F. J. Kadhim, Iraqi J. Appl. Phys. **19**, 229 (2023).
11. F. Kadhim, O. Hammadi, and N. Muthesher, J. Nanophot. **16**, 026005 (2022). DOI: 10.1117/1.JNP.16.026005.
12. S. J. Armaković, M. M. Savanović, and S. Armaković, Catalysts **13**, 26 (2023). DOI: 10.3390/catal13010026.
13. S. Sério, M. E. Melo Jorge, M. J. P. Maneira, and Y. Nunes, Mat. Chem. Phys. **126**, 73 (2011). DOI: 10.1016/j.matchemphys.2010.12.008.
14. F. a.-H. Mutlak, R. K. Jamal, and A. F. Ahmed, Iraqi J. Sci. **62**, 517 (2021). DOI: 10.24996/ijs.2021.62.2.18.
15. W. A. Al-Taa'y and B. A. Hasan, Iraqi J. Phys. **19**, 22 (2021). DOI: 10.30723/ijp.v19i49.632.
16. M. A. Hameed and Z. M. Jabbar, Iraqi J. Appl. Phys. **12**, 13 (2016).
17. H. G. Fahad and O. A. Hammadi, Iraqi J. Appl. Phys. **16**, 37 (2020).
18. Jcpds. *The International Centre for Diffraction Data (Icdd)*; https://www.icdd.com/.
19. A. Hu, X. Zhang, D. Luong, K. D. Oakes, M. R. Servos, R. Liang, S. Kurdi, P. Peng, and Y. Zhou, Was. Biom. Valoriz. **3**, 443 (2012). DOI: 10.1007/s12649-012-9142-6.
20. T. Kheamrutai, L. Pichet, and N. Boonlaer, Agricul. Nat. Res. **42**, 357 (2008).
21. N. N. Greenwood, E. J. F. Ross, and B. P. Straughan, *Index of Vibrational Spectra of Inorganic and Organometallic Compounds* (London, Butterworths, CRC Pres, 1972).
22. F. J. Al-Maliki, O. A. Hammadi, and E. A. Al-Oubidy, Iraqi J. Sci. **Special Issue**, 91 (2019). DOI: 10.24996/ijs.2019.S.I.14.
23. E. A. Al-Oubidy and F. J. Al-Maliki, Iraqi J. Appl. Phys. **14**, 19 (2018).
24. Y. Zhao, C. Li, X. Liu, F. Gu, H. Jiang, W. Shao, L. Zhang, and Y. He, Mat. Lett. **61**, 79 (2007). DOI: 10.1016/j.matlet.2006.04.010.
25. A. Zachariah, K. V. Baiju, S. Shukla, K. S. Deepa, J. James, and K. G. K. Warrier, J. Phys. Chem. C **112**, 11345 (2008). DOI: 10.1021/jp712174y.
26. I. A. Fadhl, Y. I. Al-Rikabi, M. a. H. Zaidi, A. A. Khadayeir, S. S. Chiad, and N. F. Habubi, AIP Conf. Proce. **2845**, 2845 (2023). DOI: 10.1063/5.0157094.
27. R. Singh, M. Gupta, and S. K. Mukherjee, J. Mat. Sci. Mat. Elect. **33**, 6942 (2022). DOI: 10.1007/s10854-022-07873-y.
28. S. S. Mohammed, Z. Y. Shnain, and M. F. Abid, Eng. Tech. J. **40**, 1131 (2022). DOI: 10.30684/etj.2021.131177.1015.

الخصائص التركيبيه ونشاط التحفيز الضوئي للمركب النانوي TiO_2/Si_3N_4 المحضر عبر تقنية الترذيذ بالبلازما

علي ناظم منيف[1] و فراس جواد كاظم[2]
[1]قسم الفيزياء الطبية، كليه العلوم، جامعه وارث الانبياء، كربلاء، العراق
[2]قسم الفيزياء، كليه العلوم، جامعه بغداد، بغداد، العراق

الخلاصة

يقدم هذا العمل محفزا جديدا TiO_2 / Si_3N_4 تم تحضيره عن طريق ترسيب أغشية رقيقة من التراكيب النانويةTiO2 Si3N4 على الزجاج باستخدام تقنية الاخرق المغنطرون التفاعلي DC غير المتوازنة في المختبر .تم استخدام صفائح سيليكون عالية النقاء وصفيحة تيتانيوم كهدف للرش وخليط غاز من($Ar: N_2$) ، ($Ar:O_2$) بنسب خلط (50:50) لكل منهما لتحضير عينة TiO_2 / Si_3N_4، على التوالي .تم معالجة هذه العينة بالحرارة .تم تحديد بنية وشكل المحفز من خلال حيود الأشعة السينية، والمجهر الإلكتروني الماسح ذو انبعاثات المجال (FE-SEM)، والتحليل الطيفي للأشعة السينية المشتتة للطاقة (EDX)، واختبارات التحليل الطيفي بالأشعة تحت الحمراء لتحويل فورييه (FTIR). كانت عينة المركب النانوي الناتجة متعددة البلورات ولم تكن هناك شوائب في المركب النانوي الذي تم فحصه كما كشف تحليل XRD .تم العثور على حافة الامتصاص عند $420nm^{-1}$ ، كما يتضح من التحليل الطيفي للأشعة فوق البنفسجية المرئية ، وتظهر دراسة الخصائص البصرية أيضا أن حافة امتصاص TiO_2 / Si_3N_4 قد تحولت نحو منطقة الطاقة المنخفضة (الانزياح الأحمر) بالنسبة إلى TiO_2. تشير النتائج التي تم الحصول عليها من التحلل الضوئي للملوثات العضوية تحت مصباح زينون إلى أن نشاط التحفيز الضوئي للمركب النانوي TiO_2 / Si_3N_4 أكثر فعالية بكثير من المحفز الضوئي النانوي TiO_2.

الكلمات المفتاحية: ثنائي أوكسيد التيتانيوم، نيتريد السيليكون، المتراكبات النانوية، الترذيذ التفاعلي، المحفز ضوئي.